Method of Green's Function for Characterization of SH Waves in Porous-Piezo Composite Structure with a Point Source

S. Karmakar, Sanjeev A. Sahu[*] , S. Nirwal

Department of Mathematics and Computing, Indian Institute of Technology (Indian School of Mines) Dhanbad, India

ABSTRACT

An approach of Green's function is adopted to solve the inhomogeneous linear differential equations representing wave equations in piezo-composite materials. In particular, transference of horizontally polarised shear (SH) waves is considered in bedded structure comprising of porous-piezo electric layer lying over a heterogeneous half-space. Propagation of SH-waves is considered to be influenced by point source, situated in the heterogeneous substrate. A closed form analytical solution is obtained to establish the dispersion relation. Remarkable influence of different parameters (like elastic constant, piezoelectric constant, heterogeneity parameter, initial stress and layers thickness) on the phase and group velocity are shown graphically. Moreover, a special case of present study is shown by replacing the porous piezoelectric material with piezoelectric material. Some numerical examples are illustrated by taking the material constants of Lead Zirconate Titanate (PZT-1, PZT-5H and PZT-7) for the porous piezoelectric layer where the phase velocity of SH waves is high rather than that of piezoelectric layer. © 2020 IAU, Arak Branch. All rights reserved.

Keywords: Point source; Porous piezoelectric material; Green's function; SH-waves.

1 INTRODUCTION

IN modern mobile technologies ambient light sensors have been incorporated in order to optimize the performance of display channels. In addition to this, the sensor has also been used in automobiles to accelerate the activity subsequently. SAW devices work on the principle of surface wave exists in an elastic body of free surfaces and interfaces, where the distribution is localized near the surface area. All acoustic wave devices utilize the piezoelectric effect to transduce an electric signal into a mechanical wave. The mechanical wave propagates through the material to another transducer, which converts the wave back to an electrical signal. Piezoelectric materials are extensively applicable due to the characteristic of inducing electric charge or self-polarization when subjected to a mechanical stress. It is noticed that from few decades, use of piezoelectric materials are increasing rapidly. Many

_____

[*]Corresponding author.
E-mail address: sanjeev@iitism.ac.in (Sanjeev A. Sahu).

authors have reported significant works related to piezoelectric (PE) and others material [1-8]. The boundary value problem having homogeneous boundary condition is easier to solve as compared to non-homogeneous boundary condition. The non-homogeneous boundary conditions, for which the problem has solutions, need to be homogenized with the aid of some transformations of the variable [9-10]. Green's function provides solution of elasto-dynamics problems having disturbance caused by point source. Since Green's function is a useful tool in the field of applied mathematics as it helps by providing solutions to a large number of families of differential equations. Prior to last decades, the displacement generated in a form of Love waves due to two-dimensional point source in a medium, has been studied by Ghosh et al. [11], under the scheme of Green's function. Green's function is imposed according to the material characteristics whether how it behaves mechanically to an impulsive excitation force. Many researches have solved the problem of wave propagation influenced by point source for the accepted models [12-15].PE materials are the materials, which produce electric fields subject to mechanical stress. The possible applications of PE material falls in the area of mechanical and electrical engineering, communications, geophysics (especially in making of surface wave sensors, transducers and SAW devices) [16-21]. Embedding of PE materials with composite structures forms the structures of smart material. Besides, of their enormous applications, these smart structures have many non-ignorable shortcomings. In many device applications the brittle nature of PE material, causes failure of device under mechanical and electrical loading. Such limitations can be removed by introducing porosity in a controlled fashion to the PE material as the porosity gives low material density in compare to that of previous one. PE materials containing tailored porosity are known as porous-piezoelectric materials as piezoelectric ceramics. Composition of material with porous piezoelectric ceramics reduces the brittleness fracture in the composite smart structure, which provides strength, consequently increases the efficiency of the SAW devices. Wave propagation in porous piezoelectric structure is a topic of interest nowadays. Vashishth et al. [22] have studied the wave propagation concept in porous piezoelectric materials and derived the constitutive equations. Gaur AM and Rana [23] have studied the dispersion relations for SH wave propagation in a porous piezoelectric (PZT–PVDF) composite structure. 3D waves in porous piezoelectric materials have also been studied by Vashishth and Gupta [24]. Some more literature and applications of wave propagation in PE and porous material have been found somewhere [25-29].

The present research article is confined to study the SH-wave transference (due to a point source) in porous piezoelectric layer, overlying a heterogeneous substrate. Green's function method is used to solve the governing equations. Dispersion relation is obtained analytically in closed form and matched with classical Love-wave equation. Remarkable influence of parameters like elastic constant, piezoelectric constant, heterogeneity parameter, initial stress and layers width are shown as graphically. Numerical examples are considered by acquiring the material constants of PZT-5H, PZT-7 and PZT-1 for the porous piezoelectric layer.

2   FORMULATION OF THE PROBLEM

The transference of SH wave under a point source in a framework comprising of porous piezoelectric layer (of thickness h) overlying by a heterogeneous half-space. The mathematical model specified by a Cartesian coordinate system is shown in Fig.1. Axis-y is taken along the direction of wave transference and x-axis pointing vertically downwards. A source of disturbance is located at interface 'S'. The poling direction of porous piezoelectric material is parallel to z-axis.
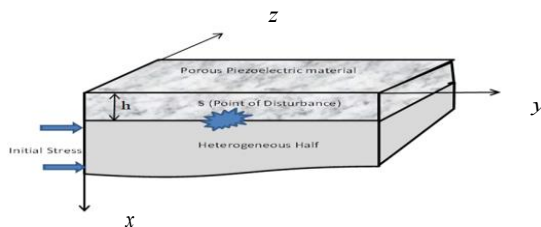

Fig.1
Geometry of the problem.

2.1 For the upper porous piezoelectric layer

The governing equation of motion for upper porous piezoelectric layer is given as:

$$\begin{cases} \breve{\sigma}^p_{ij,j} = \left(\rho^p_{11}\right)_{ij} \dfrac{\partial^2 w_j}{\partial t^2} + \left(\rho^p_{11}\right)_{ij} \dfrac{\partial^2 w^*_j}{\partial t^2}, \\[2mm] \breve{\sigma}^{pp}_{,i} = \left(\rho^p_{12}\right)_{ij} \dfrac{\partial^2 w_j}{\partial t^2} + \left(\rho^p_{22}\right)_{ij} \dfrac{\partial^2 w^*_j}{\partial t^2}, & \left(\begin{matrix}\breve{\tilde{\nabla}} = \partial_{xi} \\ i,j,k = 1,2,3\end{matrix}\right) \\[2mm] \breve{\tilde{\nabla}} \bullet \breve{D} = 0, \\[2mm] \breve{\tilde{\nabla}} \bullet \breve{D}^* = 0. \end{cases} \tag{1}$$

where, $w\left(w^*\right)$ represents the displacement components for solid (fluid) phase of the material; $\left(\rho^p_{11}\right)_{ij}, \left(\rho^p_{12}\right)_{ij}$ and $\left(\rho^p_{22}\right)_{ij}$ are the mass coefficient. The porous piezoelectric materials having the following constitutive relations

$$\begin{cases} \breve{\sigma}^P_{ij,j} = c^P_{ijkl}\, \eta^P_{kl} + \gamma^P_{ij}\, \eta^{pp} - e^P_{kij}\, E^P_k - \zeta^P_{kij}\, \xi^{pp}_k, \\[2mm] \breve{\sigma}^{pp}_{,i} = \gamma^P_{ij}\, \eta^P_{ij} + \upsilon^P\, \eta^{pp} - \zeta^{pp}_k\, E^P_k - e^{pp}_k\, \xi^{pp}_k, \\[2mm] \breve{D}^P_i = e^P_{ikj}\, \eta^P_{kl} + \zeta^{pp}_i\, \eta^{pp} + \lambda^P_{il}\, E^P_l + \theta^P_{li}\, \xi^{pp}_l, \\[2mm] \breve{D}^{pp}_{,i} = \zeta^P_{ikj}\, \eta^P_{kl} + e^{pp}_i\, \eta^{pp} + \theta^P_{il}\, E^P_l + \lambda^{pp}_{il}\, \xi^{pp}_l. \end{cases} \tag{2}$$

where $c^P_{ijkl}, \gamma^P_{ij}$ and υ^p represent the elastic constants; $\lambda^P_{il}, \theta^P_{li}$ and λ^{pp}_{il} represent the dielectric constants; $\eta^P_{kl}\left(\eta^P\right), \breve{\sigma}^P_{ij,j}\left(\breve{\sigma}^{pp}_{,i}\right), \breve{D}^P_i\left(\breve{D}^{pp}_{,i}\right)$ and $E^P_k\left(\xi^{pp}_k\right)$ are the strain tensor, stress tensor, electric displacement and electric field for solid (fluid) phase of the material, respectively. The relation between strain tensors, displacement components, electric fields and electric potentials are as:

$$\eta^P_{ij} = 0.5\left(w_{i,j} + w_{j,i}\right), \quad \eta^{pp} = w^*_{i,i}, \quad E^P_i = -\phi_{,i}, \quad \zeta^{pp}_i = -\varphi_{,i}. \tag{3}$$

where, $\phi(\varphi)$ represents the electric potential function for solid (fluid) phase of the material. We have considered that the wave propagates along y-axis, the displacement and electric potential function (for solid and fluid phase) can be defined as:

$$u = v = 0, w = w^P_1\left(x,y,t\right), w^* = w^{pp}_1\left(x,y,t\right), \phi = \phi^P_1\left(x,y,t\right), \varphi = \varphi^{pp}_1\left(x,y,t\right). \tag{4}$$

On substituting the values from Eqs. (3) and (4) in Eq. (2), we get

$$\begin{cases} \breve{\sigma}^P_{xz} = c^P_{44}\, \dfrac{\partial w^P_1}{\partial x} + e^P_{15}\, \dfrac{\partial \phi^P_1}{\partial x} + \zeta^P_{15}\, \dfrac{\partial \varphi^{pp}_1}{\partial x}, \\[2mm] \breve{\sigma}^P_{yz} = c^P_{44}\, \dfrac{\partial w^P_1}{\partial y} + e^P_{15}\, \dfrac{\partial \phi^P_1}{\partial y} + \zeta^P_{15}\, \dfrac{\partial \varphi^{pp}_1}{\partial y}, \\[2mm] \breve{D}^P_1 = e^P_{15}\, \dfrac{\partial w^P_1}{\partial x} + \lambda^P_{11}\, \dfrac{\partial \phi^P_1}{\partial x} + \theta^P_{11}\, \dfrac{\partial \varphi^{pp}_1}{\partial x}, \\[2mm] \breve{D}^P_2 = e^P_{15}\, \dfrac{\partial w^P_1}{\partial y} + \lambda^P_{11}\, \dfrac{\partial \phi^P_1}{\partial y} + \theta^P_{11}\, \dfrac{\partial \varphi^{pp}_1}{\partial y}, \\[2mm] \breve{D}^P_1 = \zeta^P_{15}\, \dfrac{\partial w^P_1}{\partial x} - \theta^P_{11}\, \dfrac{\partial \phi^P_1}{\partial x} - \lambda^{pp}_{11}\, \dfrac{\partial \varphi^{pp}_1}{\partial x}, \\[2mm] \breve{D}^{pp}_2 = \zeta^P_{15}\, \dfrac{\partial w^P_1}{\partial y} - \theta^P_{11}\, \dfrac{\partial \phi^P_1}{\partial y} - \lambda^{pp}_{11}\, \dfrac{\partial \varphi^{pp}_1}{\partial y}. \end{cases} \tag{5}$$

Let $\psi_1(r,t)$ be the distribution of force density in the upper layer due to point source at the common interface; r is the distance from the origin (where the force is applied to a point of coordinates) and t is time. With the help of Eq. (1) and (5), we get

$$c_{44}^p\left(\frac{\partial^2 w_1^{\,P}}{\partial x^{\,2}}+\frac{\partial^2 w_1^{\,P}}{\partial y^{\,2}}\right)+e_{15}^{\Delta p}\left(\frac{\partial^2 \phi_1^{p}}{\partial x^{\,2}}+\frac{\partial^2 \phi_1^{p}}{\partial y^{\,2}}\right)+\zeta_{15}^{\Delta p}\left(\frac{\partial^2 \varphi_1^{pp}}{\partial x^{\,2}}+\frac{\partial^2 \varphi_1^{pp}}{\partial y^{\,2}}\right)=\rho_1^p\frac{\partial^2 w_1^{\,P}}{\partial t^{\,2}}+4\pi\,\psi_1(r,t) \tag{6a}$$

$$e_{15}^p\left(\frac{\partial^2 w_1^{\,P}}{\partial x^{\,2}}+\frac{\partial^2 w_1^{\,P}}{\partial y^{\,2}}\right)-\lambda_{11}^p\left(\frac{\partial^2 \phi_1^{p}}{\partial x^{\,2}}+\frac{\partial^2 \phi_1^{p}}{\partial y^{\,2}}\right)-\theta_{11}^p\left(\frac{\partial^2 \varphi_1^{pp}}{\partial x^{\,2}}+\frac{\partial^2 \varphi_1^{pp}}{\partial y^{\,2}}\right)=0 \tag{6b}$$

$$\zeta_{15}^{\Delta p}\left(\frac{\partial^2 w_1^{\,P}}{\partial x^{\,2}}+\frac{\partial^2 w_1^{\,P}}{\partial y^{\,2}}\right)-\theta_{11}^{\Delta p}\left(\frac{\partial^2 \phi_1^{p}}{\partial x^{\,2}}+\frac{\partial^2 \phi_1^{p}}{\partial y^{\,2}}\right)-\lambda_{11}^{\Delta pp}\left(\frac{\partial^2 \varphi_1^{pp}}{\partial x^{\,2}}+\frac{\partial^2 \varphi_1^{pp}}{\partial y^{\,2}}\right)=0, \tag{6c}$$

where, $\rho_1^p=\left(\rho_{11}^p\right)_{33}-\dfrac{\left[\left(\rho_{12}^p\right)^2\right]_{33}}{\left(\rho_{22}^p\right)_{33}}.$

Moreover, rearranging the Eq. (6), we get

$$\hat{c}_{44}^p\left(\frac{\partial^2 w_1^{\,P}}{\partial x^{\,2}}+\frac{\partial^2 w_1^{\,P}}{\partial y^{\,2}}\right)+\hat{e}_{15}^p\left(\frac{\partial^2 \phi_1^{p}}{\partial x^{\,2}}+\frac{\partial^2 \phi_1^{p}}{\partial y^{\,2}}\right)=\rho_1^p\frac{\partial^2 w_1^{\,P}}{\partial t^{\,2}}+4\pi\psi_1(r,t) \tag{7a}$$

$$\hat{e}_{15}^p\left(\frac{\partial^2 w_1^{\,P}}{\partial x^{\,2}}+\frac{\partial^2 w_1^{\,P}}{\partial y^{\,2}}\right)-\hat{\lambda}_{11}^p\left(\frac{\partial^2 \phi_1^{p}}{\partial x^{\,2}}+\frac{\partial^2 \phi_1^{p}}{\partial y^{\,2}}\right)=0 \tag{7b}$$

$$\left(\frac{\partial^2 \varphi_1^{pp}}{\partial x^{\,2}}+\frac{\partial^2 \varphi_1^{pp}}{\partial y^{\,2}}\right)=\frac{1}{\lambda_{11}^{pp}}\left(\zeta_{15}^p\left(\frac{\partial^2 w_1^{\,P}}{\partial x^{\,2}}+\frac{\partial^2 w_1^{\,P}}{\partial y^{\,2}}\right)-\theta_{11}^p\left(\frac{\partial^2 \phi_1^{p}}{\partial x^{\,2}}+\frac{\partial^2 \phi_1^{p}}{\partial y^{\,2}}\right)\right) \tag{7c}$$

where, $\hat{c}_{44}^p=c_{44}^p+\dfrac{\left(\zeta_{15}^p\right)^2}{\lambda_{11}^{pp}}$, $\hat{e}_{15}^p=e_{15}^p-\dfrac{\theta_{11}^p\,\zeta_{15}^p}{\lambda_{11}^{pp}}$ and $\hat{\lambda}_{11}^p=\lambda_{11}^p-\dfrac{\left(\theta_{11}^p\right)^2}{\lambda_{11}^{pp}}$, .

Let us suppose that the solutions of Eq. (7) are

$$w_1^{\,P}(x,y,t)=\bar{w}_1^{\,P}(x,y)e^{i\varpi t},\ \phi_1^p(x,y,t)=\bar{\phi}_1^p(x,y)e^{i\varpi t},\ \varphi_1^{pp}(x,y,t)=\bar{\varphi}_1^{pp}(x,y)e^{i\varpi t},\ \psi_1(r,t)=\bar{\psi}_1(r)e^{i\varpi t}. \tag{8}$$

Due to the impulsive force, the disturbance can be represented in the form of Dirac-delta function at the source point as $\bar{\psi}(r)=\delta(y)\delta(x-h)$. Now, let us introduce the new functions $W_1^p(\Gamma,x)$, $\Phi_1^p(\Gamma,x)$ and $\Theta_1^{pp}(\Gamma,x)$. Suppose that the functions $W_1^p(\Gamma,x)$, $\Phi_1^p(\Gamma,x)$ and $\Theta_1^{pp}(\Gamma,x)$ are the Fourier transformation of $\bar{w}_1^p(x,y)$, $\bar{\phi}_1^p(x,y)$ and $\bar{\varphi}_1^{pp}(x,y)$ respectively, we have

$$\begin{cases} W_1^p(\Gamma,x)=\dfrac{1}{2\pi}\displaystyle\int_{-\infty}^{\infty}\bar{w}_1^p(x,y)e^{i\Gamma y}\,dy, \\[3mm] \Phi_1^p(\Gamma,x)=\dfrac{1}{2\pi}\displaystyle\int_{-\infty}^{\infty}\bar{\phi}_1^p(x,y)e^{i\Gamma y}\,dy, \\[3mm] \Theta_1^{pp}(\Gamma,x)=\dfrac{1}{2\pi}\displaystyle\int_{-\infty}^{\infty}\bar{\varphi}_1^{pp}(x,y)e^{i\Gamma y}\,dy. \end{cases} \tag{9}$$

Moreover, the inverse Fourier transformation functions

$$
\begin{cases}
\overline{w}_1^p(x,y)=\int_{-\infty}^{\infty} W_1^p(\Gamma,x)e^{-i\Gamma y}\,d\Gamma, \\
\overline{\phi}_1^p(x,y)=\int_{-\infty}^{\infty} \Phi_1^p(\Gamma,x)e^{-i\Gamma y}\,d\Gamma, \\
\overline{\varphi}_1^{pp}(x,y)=\int_{-\infty}^{\infty} \Theta_1^{pp}(\Gamma,x)e^{-i\Gamma y}\,d\Gamma.
\end{cases}
\tag{10}
$$

By applying the Fourier transformation on Eq. (7), we get the following ordinary differential equations of second order

$$
\hat{c}_{44}^p\left(\frac{d^2 W_1^p}{dx^2}-\Gamma^2 W_1^{\Delta p}\right)+\hat{e}_{15}^p\left(\frac{d^2 \Phi_1^p}{dx^2}-\Gamma^2\Phi_1^p\right)-\rho_1^p\varpi^2 W_1^p=2\delta(x-h),
\tag{11a}
$$

$$
\hat{e}_{15}^p\left(\frac{d^2 W_1^p}{dx^2}-\Gamma^2 W_1^p\right)-\hat{\lambda}_{11}^p\left(\frac{d^2\Phi_1^p}{dx^2}-\Gamma^2\Phi_1^p\right)=0,
\tag{11b}
$$

$$
\left(\frac{d^2\Theta_1^{pp}}{dx^2}-\Gamma^2\Theta_1^{pp}\right)=\frac{1}{\lambda_{11}^p}\left[\zeta_{15}^p\left(\frac{dW_1^p}{dx^2}-\Gamma^2 W_1^{\Delta p}\right)-\theta_{11}^p\left(\frac{d^2\Phi_1^p}{dx^2}-\Gamma^2\Phi_1^p\right)\right],
\tag{11c}
$$

where, $\psi_1(r)=\delta(y)\delta(x-h)$. Now, from Eqs. 11(a) and 11(b), we have

$$
\frac{d^2 W_1^p}{dx^2}-v_1^2 W_1^p=4\pi\psi_1(x),
\tag{12}
$$

where, $v_1^2=\Gamma^2-\dfrac{\rho_1\varpi^2}{\ell_1}$ and $\psi_1(x)=\dfrac{1}{2\pi}\dfrac{\delta(x-h)}{\ell_1}$ with $\ell_1=\hat{c}_{44}^p+\dfrac{\left(\hat{e}_{15}^p\right)^2}{\hat{\lambda}_{11}^p}$.

2.2 For the pre-stressed heterogeneous substrate

The equation of motion for pre-stressed heterogeneous substrate can be written as:

$$
\frac{\partial}{\partial y}\left[\left(\mu^*-\frac{\sigma}{2}\right)\frac{\partial w_2^h}{\partial y}\right]+\frac{\partial}{\partial x}\left(\mu^*\frac{\partial w_2^h}{\partial x}\right)=\rho_2^h\frac{\partial w_2^h}{\partial t^2},
\tag{13}
$$

where, σ, ρ_2^h and μ^* represent the initial stress, density and rigidity of the material respectively. We have assumed heterogeneity associated with rigidity in half-space and varies linearly.

$$
\mu^*=\mu+\gamma(x-h)
\tag{14}
$$

where, γ is the heterogeneity parameter and μ is the rigidity of the substrate. Let us assume the solutions of Eq. (13) can

$$
w_2^h(x,y,t)=\overline{w}_2^h(x,y)e^{i\varpi t},
\tag{15}
$$

On substituting the values from Eqs. (14) and (15) in Eq. (13), we get

$$\left(\mu-\frac{\sigma}{2}\right)\frac{\partial^2\bar{w}_2^{\,h}}{\partial y^2}+\mu\frac{\partial^2\bar{w}_2^{\,h}}{\partial x^2}-\rho_2^h\frac{\partial^2\bar{w}_2^{\,h}}{\partial t^2}=-\gamma(x-h)\frac{\partial^2\bar{w}_2^{\,h}}{\partial t^2}-\gamma(x-h)\frac{\partial\bar{w}_2^{\,h}}{\partial x^2}-\gamma\frac{\partial\bar{w}_2^{\,h}}{\partial x}$$

(16)

Now, let us introduce the function $W_2^{\,h}(\Gamma,x)$. Suppose that the functions $W_2^{\,h}(\Gamma,x)$ are the Fourier transformation of $\bar{w}_2^{\,h}(x,y)$, then,

$$W_2^{\,h}(\Gamma,x)=\frac{1}{2\pi}\int_{-\infty}^{\infty}\bar{w}_2^{\,h}(x,y)e^{i\Gamma y}\,dy.$$

(17)

Moreover, there inverse Fourier transformation

$$\bar{w}_2^{\,h}(x,y)=\int_{-\infty}^{\infty}W_2^{\,h}(\Gamma,x)e^{-i\Gamma y}\,d\Gamma.$$

(18)

By applying the Fourier transformation on Eq. (16), we get the following ordinary differential equation of second order

$$\frac{d^2W_2^{\,h}}{dx^2}-v_2^2W_2^{\,h}=4\pi\psi_2(x).$$

(19)

where, $v_2^2=\left(1-\frac{\sigma}{2\mu}\right)\Gamma^2-\frac{\rho_2\varpi^2}{\mu}$ and $4\pi\psi_2(x)=\frac{-\gamma(\tilde{x}-h)}{\mu}\frac{d^2W_2^{\,h}}{dx^2}+\frac{\gamma(x-h)\Gamma^2W_2^{\,h}}{\mu}-\frac{\gamma}{\mu}\frac{dW_2^{\,h}}{dx}$

3 BOUNDARY CONDITIONS AND APPRAISAL OF CONSTANTS

In order to find the solutions of Eqs. (13) and (19), we use the Green's Function approach along with the following boundary conditions:

I.   The mechanical traction free and electrical boundary conditions (both open and closed circuit case) at the free surface are

$(a)\,\sigma_{zx}^p(x)=0,$ $(b)\,D_x^p(x)+D_x^{pp}(x)=0,$

$(c)\,\Phi_1^p(x)=0,$ $(d)\,\Theta_1^{pp}(x)=0.$

II.   The continuity conditions at the common interface of the upper layer and substrate are

$(e)\,\sigma_{zx}^p(x)=\sigma_{zx}^h(x),$

$(g)\,W_1^{\,p}(x)=W_1^{\,h}(x),$ $(f)\,D_{\tilde{x}}^p(x)+D_x^{pp}(x)=0,$

$(i)\,\Theta_1^{pp}(x)=0.$ $(h)\,\Phi_1^p(x)=0,$

Now, using the above conditions (a), (b), (e) and (f), we can represent the boundary conditions

$$\frac{dW_1^{\,p}}{dx}=0 \qquad \text{at} \quad x=0,$$

(20)

$$c_{44}^p \frac{dW_1^{\,p}}{dx} = \mu \frac{dW_2^{\,h}}{dx} \qquad \text{at} \quad x = h.$$ (21)

Let us consider $G_1(x/x_\circ)$ be the Green's function (in the context of upper porous-piezoelectric layer) that satisfies the following condition

$$\frac{dG_1(x/x_\circ)}{dx} = 0 \text{ at } x = 0 \text{ and } h,$$ (22)

where, $x_\circ$ is an arbitrary point of the upper layer. Green's function $G_1(x/x_\circ)$ will also satisfy the following condition

$$\frac{d^2 G_1(x/x_\circ)}{dx^2} - v_1^2 G_1(x/x_\circ) = \delta(x - x_\circ).$$ (23)

On multiplying Eq. (12) by $G_1(x/x_\circ)$ and Eq. (23) by W_1^p and then subtracting, we have

$$G_1(x/x_\circ)\frac{d^2 W_1^{\,p}}{dx^2} - W_1^p \frac{d^2 G_1(x/x_\circ)}{dx^2} = 4\pi\psi_1(x)G_1(x/x_\circ)dx - \delta(x - x_\circ)W_1^p dx.$$ (24)

Now, on integrating Eq. (24) with respect to x between the limits $x = 0$ and h, we get

$$\int_{x=0}^{x=h}\left[G_1(x/x_\circ)\frac{dW_1^{\,p}}{dx^2} - W_1^p \frac{dG_1(x/x_\circ)}{dx^2} \right]dx = \int_{x=0}^{x=h}\left[4\pi\psi_1(x)G_1(x/x_\circ) - \delta(x - x_\circ)W_1^p \right]dx.$$

On using the Eq. (22), we can write

$$G_1(h/x_\circ)\frac{d^2 W_1^{\,p}}{dx^2}\bigg|_{\hat{x}=h} = \frac{2}{\ell_1}G_1(h/x_\circ) - W_1^p(x_\circ).$$ (25)

On replacing the variable $x_\circ$ by x in Eq. (25), the expression of displacement function for the upper layer at arbitrary point as:

$$W_1^p(x) = \frac{2}{\ell_1}G_1(x/h) - G_1(x/h)\frac{dW_1^{\,p}}{dx}\bigg|_{x=h},$$ (26)

where, $G_1(h/x) = G_1(x/h)$. Similarly, let $G_2(x/x_\circ)$ be the Green's function (in the context of lower heterogeneous half- space) which satisfies the following condition

$$\frac{dG_2(x/x_\circ)}{dx} = 0 \text{ at } x = h$$ (27)

$$\frac{dG_2(x/x_\circ)}{dx} \to 0 \ as \ x \to \infty$$ (28)

Green's function $G_2(x/x_\circ)$ will also satisfy the following condition

$$\frac{d^2G_2(x/x_\circ)}{dx^2} - v_2^2 G_2(x/x_\circ) = \delta(x - x_\circ),$$ (29)

where $x_\circ$ is an arbitrary point of half space. On multiplying Eq. (19) by $G_2(x/x_\circ)$ and Eq. (29) by W_2^h and on subtracting, we get

$$G_2(x/x_\circ)\frac{d^2W_2^h}{dx^2} - W_2^h \frac{dG_2(x/x_\circ)}{dx^2}dx = 4\pi\psi_2(x)G_2(x/x_\circ)dx - \delta(x-x_\circ)W_2^h dx.$$ (30)

Now, on integrating Eq. (30) with respect to x between the limits $x = 0$ and ∞, we get

$$\int\limits_{x=h}^{x=\infty}\left[G_2(x/x_\circ)\frac{d^2W_2^h}{dx^2} - W_2^h \frac{d^2G_2}{dx^2}(x/x_\circ)\right]dx = \int\limits_{x=h}^{x=\infty}\left[4\pi\psi_2(x)G_2(x/x_\circ) - \delta(x-x_\circ)W_2^h\right]dx,$$

which reduces to

$$-G_2(h/x_\circ)\frac{d^2W_2^h}{dx^2}\Bigg|_{x=h}^{x=\infty} = \int\limits_{x=h}^{x=\infty} 4\pi\psi_2(x)G_2(x/x_\circ)dx - W_2^h(x_\circ).$$ (31)

On replacing $x_\circ$ by x in Eq. (31), then, the expression of displacement function for the lower half space at arbitrary point as:

$$W_2^h(x) = \int\limits_{x=h}^{x=\infty} 4\pi\psi_2(x_\circ)G_2(x/x_\circ)dx + G_2(x/h)\frac{dW_2^h}{dx}\Bigg|_{x=h},$$ (32)

where $G_2(h/x) = G_2(x/h)$ and $G_2(x_\circ/x) = G_2(x/x_\circ)$. By using boundary condition (II. g) and Eqs. (20), (21) and (32), we have

$$\frac{dW_1^p}{dx}\Bigg|_{x=h} = \frac{2\mu G_1(h/h)}{\ell_1\left(\mu G_1(h/h) + c_{44}^p G_2(h/h)\right)} - \frac{\mu}{\left(\mu G_1(h/h) + c_{44}^p G_2(h/h)\right)}\int\limits_{x_\circ=h}^{x_\circ=\infty} 4\pi\psi_2(x_\circ)G_2(h/x_\circ)dx_\circ.$$

Substituting the following value in Eq. (26), we get

$$W_1^p = \frac{2}{\ell_1}\frac{G_1(x/h)G_2(h/h)}{\mu G_1(h/h) + c_{44}^p G_2(h/h)} - \frac{2\mu G_1(x/h)G_1(h/h)}{\ell_1\left(\mu G_1(h/h) + c_{44}^p G_2(h/h)\right)}\times\int\limits_{x_\circ=h}^{x_\circ=\infty} 4\pi\psi_2(x_0)G_2(h/x_\circ)dx_\circ.$$ (33)

Moreover, on using the value of $4\pi\psi_2(x)$ from Eq. (19),

$$W_1^p = \frac{2c_{44}^p}{\ell_1}\frac{G_1(x/h)G_2(h/h)}{\mu G_1(h/h) + c_{44}^p G_2(h/h)} - \frac{2\gamma G_1(x/h)G_1(h/h)}{\mu G_1(h/h) + c_{44}^p G_2(h/h)}\times$$
$$\int\limits_{x_\circ=h}^{x_\circ=\infty}\left\{(x_\circ - h)\frac{d^2W_2^h}{dx^2} - (x_\circ - h)\Gamma^2 W_2^h + d_x W_2^h\right\}G_2(h/x_\circ)dx_\circ.$$ (34)

Similarly with the help of Eqs. (21) and (32), the displacement function for first approximation (neglect the higher power of γ)

$$W_2^p = \frac{2c_{44}^p}{\ell_1} \frac{G_2(x/h)G_1(h/h)}{\mu G_1(h/h) + c_{44}^p G_2(h/h)}. \tag{35}$$

On substituting the value from Eq. (35) in Eq. (34), we get

$$W_1^p = \frac{2c_{44}^p}{\ell_1} \frac{G_1(x/h)G_2(h/h)}{\mu G_1(h/h) + c_{44}^p G_2(h/h)} - \frac{2c_{44}^p}{\ell_1} \frac{\gamma G_1(x/h)G_1(h/h)}{\left(\mu G_1(h/h) + c_{44}^p G_2(h/h)\right)^2} \times$$

$$\int_{x_\circ = h}^{x_\circ = \infty} \left\{ (x_\circ - h)\frac{d^2 G_2(x_\circ/h)}{dx^2} - (x_\circ - h)\Gamma^2 G_2(x_\circ/h) + \frac{dG_2(x_\circ/h)}{dx} \right\} G_2(h/x_\circ) dx_\circ \tag{36}$$

The displacements are the function of G_i, so it is necessary to find the values of Green's function to obtain the value of displacement. From Eq. (23), we can write

$$\frac{d^2 G\left(x/x_0\right)}{dx^2} - v_1^2 G\left(x/x_0\right) = 0. \tag{37}$$

Let P_1 and P_2 be two independent solutions of Eq. (37) vanish at $x = -\infty$ and ∞ respectively, then $P_1(x) = e^{v_1 x}$ and $P_2(x) = e^{-v_1 x}$. Then the solutions of Eq. (37) for an infinite medium are

$$\begin{cases} \dfrac{P_1(x)P_2(x_\circ)}{\omega} & \text{for } x < x_\circ \\ \dfrac{P_1(x_\circ)P_2(x)}{\omega} & \text{for } x > x_\circ \end{cases} \quad \text{where } \omega = P_1(x)\frac{dP_2(x)}{dx} - P_2(x)\frac{dP_1(x)}{dx} = -2v_1.$$

In a simplified way the solutions of Eq. (37) for an infinite medium is $\dfrac{-e^{-v_1|x-x_\circ|}}{2v_1}$. Moreover, with the help of Eq. (22), we get

$$G_1(x/x_\circ) = \frac{1}{2v_1}\left(e^{-v_1|x-x_\circ|}\right) + \frac{1}{2v_1}\left[\frac{\left(e^{v_1 x}\left\{e^{-v_1(h+x_\circ)} + e^{-v_1(h-x_\circ)}\right\} + e^{-v_1 x}\left\{e^{v_1(h-x_\circ)} + e^{-v_1(h-x_\circ)}\right\}\right)}{e^{v_1 h} - e^{-v_1 h}}\right]$$

$$G_2(x/x_\circ) = \frac{1}{2v_2}\left[e^{-v_2|x-x_\circ|} + e^{-v_2|x+x_\circ-2h|}\right] \tag{38}$$

4   DISPERSION RELATION

On substituting the values from Eq. (38) in Eqs. (35) and (36), we get

$$W_1^p = \frac{-2c_{44}^p\left(e^{-v_1 x} + e^{v_1 x}\right)}{\left(e^{v_1 h}\left\{\mu v_2 + v_1 c_{44}^p\right\} - e^{-v_1 h}\left\{-\mu v_2 + v_1 c_{44}^p\right\}\right)\ell_1} + \frac{2\gamma c_{44}^p\left(\dfrac{1}{2} + \dfrac{\Gamma^2}{4(v_2)^2}\right)\left(e^{-v_1 x} + e^{v_1 x}\right)\left(e^{v_1 h} + e^{-v_1 h}\right)}{\ell_1\left(e^{v_1 h}\left\{\mu v_2 + v_1 c_{44}^p\right\} - e^{-v_1 h}\left\{-\mu v_2 + v_1 c_{44}^{\Delta p}\right\}\right)}. \tag{39}$$

Eq. (39) has been further simplified to yield the given result

$$W_1^p = \frac{-2\left(e^{-v_1 x} + e^{v_1 x}\right)}{\left(e^{v_1 h}\left\{\mu v_2 + v_1 c_{44}^p\right\} - e^{-v_1 h}\left\{-\mu v_2 + v_1 c_{44}^p\right\}\right)} \frac{c_{44}^p}{\ell_1} \left[\frac{1}{1 + \dfrac{\gamma\left(\dfrac{1}{2} + \dfrac{\Gamma^2}{4(v_2)^2}\right)\left(e^{v_1 h} + e^{-v_1 h}\right)}{\left(e^{v_1 h}\left\{\mu v_2 + v_1 c_{44}^p\right\} - e^{-v_1 h}\left\{-\mu v_2 + v_1 c_{44}^p\right\}\right)}}\right]. \tag{40}$$

Eq. (40) contained the heterogeneity parameter (γ), assuming the value of γ small, we neglect the higher power term. So by using inverse Fourier transformation, the displacement at arbitrary point for upper porous piezoelectric layer is

$$w_1^p = \left(\frac{-2c_{44}^p}{\ell_1}\right) \int_{-\infty}^{\infty} \left(\frac{\left(e^{-v_1 x} + e^{v_1 x}\right)}{\left(e^{v_1 h}\left\{\mu v_2 + v_1 c_{44}^p\right\} - e^{-v_1 h}\left\{-\mu v_2 + v_1 c_{44}^p\right\}\right) + \gamma\left(1 + \dfrac{\Gamma^2}{2(v_2)^2}\right) Cos\, h\left(h v_1\right)}\right) e^{-i\Gamma x}\, d\Gamma, \tag{41}$$

where the factor of time is omitted. Now we will compute electric potential (for both solid and fluid phase). Let us assume that

$$\Upsilon\left(x, y, t\right) = \Phi_1^p\left(x, y, t\right) - \frac{e_{15}^{pp}}{\zeta_{11}^{pp}} W_1^p\left(x, y, t\right). \tag{42}$$

On substituting the value from Eq. (42) in Eq. (11b), then the electric potential function for the solid phase of porous piezoelectric material are

$$\Phi_1^p\left(x, y, t\right) = A_3 e^{-\Gamma x} + A_4 e^{\Gamma x} + \frac{e_{15}^{pp}}{\zeta_{11}^{pp}} \frac{2\left(e^{-v_1 x} + e^{v_1 x}\right)}{\left(e^{v_1 h}\left\{\mu v_2 + v_1 c_{44}^p\right\} - e^{-v_1 h}\left\{-\mu v_2 + v_1 c_{44}^p\right\}\right)} \times$$

$$\left(1 - \frac{\gamma\left(\dfrac{1}{2} + \dfrac{\Gamma^2}{4(v_2)^2}\right)\left(e^{v_1 h} + e^{-v_1 h}\right)}{\left(e^{v_1 h}\left\{\mu v_2 + v_1 c_{44}^p\right\} - e^{-v_1 h}\left\{-\mu v_2 + v_1 c_{44}^p\right\}\right)}\right). \tag{43}$$

On using the boundary condition (c) and (h), we get

$$\phi_1^p\left(x, y, t\right) = \frac{-2 e_{15}^{pp} c_{44}^p}{\zeta_{11}^{pp} Sin\, h(\Gamma_1 h)\ell_1} \left[1 - \frac{\gamma\left(1 + \dfrac{\Gamma^2}{2(v_2)^2}\right)\left(e^{v_1 h} + e^{-v_1 h}\right)}{\left(e^{v_1 h}\left\{\mu v_2 + v_1 c_{44}^p\right\} - e^{-v_1 h}\left\{-\mu v_2 + v_1 c_{44}^p\right\}\right)}\right] *$$

$$\left[2\left(e^{\Gamma(x-h)} - e^{-\Gamma(x-h)}\right) - \left(e^{(v_1 h + \Gamma x)} - e^{-(v_1 h + \Gamma x)}\right) - \left(e^{(-v_1 h + \Gamma x)} - e^{-(-v_1 h + \Gamma x)}\right) + \left(e^{v_1 x} + e^{-v_1 x}\right)\right]. \tag{44}$$

By using inverse Fourier transformation of Eq. (44), the electric potential (solid phase) at an arbitrary point for upper layer are

$$\phi_1^{\Delta p} = \frac{-2e_{15}^{pp}c_{44}^{\Delta p}}{\varsigma_{11}^{pp}\ell_1}\int_{-\infty}^{\infty}\frac{\begin{bmatrix}2\left(e^{\Gamma(x-h)}-e^{-\Gamma(x-h)}\right)-\left(e^{(v_1h+\Gamma x)}-e^{-(v_1h+\Gamma x)}\right)\\-\left(e^{(-v_1h+\Gamma\tilde{x})}-e^{-(-v_1h+\Gamma\tilde{x})}\right)+\left(e^{v_1\tilde{x}}+e^{-v_1\tilde{x}}\right)\end{bmatrix}e^{-i\Gamma x}}{\left[\left(e^{v_1h}\left\{\mu v_2+v_1c_{44}^{p}\right\}-e^{-v_1h}\left\{-\mu v_2+v_1c_{44}^{p}\right\}\right)-\gamma\left(1+\frac{\Gamma^2}{2(v_2)^2}\right)\text{Cos h}(hv_1)\right]\text{Sin h}(\Gamma h)}d\Gamma.\qquad(45)$$

Similarly, we can find the electric potential for fluid phase at arbitrary point. By solving the integral of Displacement and electric potentials function (fluid and solid phase) for poles, we get the following equation

$$\left(e^{v_1h}\left\{\mu v_2+v_1c_{44}^{p}\right\}-e^{-v_1h}\left\{-\mu v_2+v_1c_{44}^{p}\right\}\right)+\gamma\left(1+\frac{\Gamma^2}{2(v_2)^2}\right)\text{Cos h}(hv_1)=0.\qquad(46)$$

Eq. (46) is the dispersion relation of SH wave propagating in the porous-piezo composite structure under the influence of point source which is lying over a pre-stressed heterogeneous half space.

Replacing v_1 by iv_1 and Γ by k, we get

$$Tan\,v_1^0 h = \frac{\mu\sqrt{\left(1-\frac{\sigma}{2\mu}\right)-\frac{c^2}{\beta_2^2}}}{c_{44}^{p}\sqrt{\frac{c^2}{\beta_1^2}-1}}+\frac{\gamma}{2k\left(c_{44}^{p}\right)\sqrt{\frac{c^2}{\beta_1^2}-1}}\left(1+\frac{k^2}{2k^2\left(\left(1-\frac{\sigma}{2\mu}\right)-\frac{c^2}{\beta_2^2}\right)}\right)\qquad(47)$$

$$i\,v_1 = v_1^0 = \sqrt{\frac{c^2}{\beta_1^2}-1},\quad \beta_1^2=\frac{1}{\rho_1}\left(\hat{c}_{44}^{p}+\frac{\left(\hat{e}_{15}^{p}\right)^2}{\hat{\lambda}_{11}^{p}}\right),\quad \beta_2^2=\frac{\mu}{\rho_2}.$$

5   SPECIAL CASES AND VALIDATION

Case I
When the considered geometry reduces to transversally isotropic with initial stress , with point source, then the dispersion relation becomes [14]

$$Tankh\left(\sqrt{\frac{c^2}{\beta_1^2}-1}\right)=\frac{\mu\sqrt{\left(1-\beta_2^2\right)-\frac{c^2}{\beta_2^2}}}{\mu_1\sqrt{\frac{c^2}{\beta_1^2}-1-\frac{\sigma_1}{2\mu_1}}}+\frac{\gamma h}{2\mu_1}\frac{\left[1+\frac{1}{2}\left(\frac{\beta_2^2}{c^2}\left\{1-\beta_2^2\right\}-1\right)^{-1}\right]}{kh\left(\frac{c^2}{\beta_1^2}-1\right)^{\frac{1}{2}}}\quad\text{where }c_{44}^{\Delta p}=\mu_1.$$

Case II
When the considered geometry reduces to transversely isotropic layer lying over a transversely isotropic elastic material with a point source, then the dispersion relation becomes [31]

$$Tankh\left(\sqrt{\frac{c^2}{\beta_1^2}-1}\right)=\frac{\mu_2\sqrt{1-\frac{c^2}{\beta_2^2}}}{\mu_1\sqrt{\frac{c^2}{\beta_1^2}-1}}-\frac{\gamma h}{4\mu_1}\frac{\left(\frac{c^2}{\beta_1^2}\right)}{\left(\frac{c^2}{\beta_1^2}-1\right)kh\left(\frac{c^2}{\beta_1^2}-1\right)^{\frac{1}{2}}}$$

Case III
When the considered geometry reduces to transversally isotropic with then the dispersion relation becomes

$$Tan\left(kh\left(\sqrt{\frac{c^2}{\beta_1^2}-1}\right)\right)=\frac{\mu\sqrt{1-\frac{c^2}{\beta_2^2}}}{\mu_1\sqrt{\frac{c^2}{\beta_1^2}-1}}, \ \beta_1^2=\frac{\mu_1}{\varsigma_1}, \ \beta_2^2=\frac{\mu}{\varsigma_2} \ ,\text{where } c_{44}^{\Delta p}=\mu_1,$$

which is a classical Love-wave equation [15].

6 GROUP VELOCITY

The group velocity refers to the speed at which the whole group of waves travel. The variation of group velocity (c_g) expresses the rate at which energy is transported. The group velocity can be calculated by the formula $c_g=d_k\varpi=c+k\,d_k c$, where ϖ is the frequency of wave, k is the wave number and c is the phase velocity.

If the group velocity is greater than the speed of phase velocity, the dispersion is termed as 'anomalous' otherwise 'normal'.

7 NUMERICAL EXAMPLE AND DISCUSSIONS

To show the impact of different parameters on the phase and group velocity, numerical examples are provided. We have considered the elastic constants of Lead Zirconate Titanate (PZT-1, PZT-5H, PZT-7) for porous-piezoelectric medium. The material constants for the porous piezoelectric layer and heterogeneous half space are given in Tables 1 and 2 respectively.

Table1
Material Constants for porous piezoelectric material. [32]

Parameter /Materials	PZT-1	PZT-5H	PZT-7
$\left(\varsigma_{11}^p\right)_{33}/\left(kg\cdot m^{-3}\right)$	4950	4950	4950
$\left(\varsigma_{12}^p\right)_{33}/\left(kg\cdot m^{-3}\right)$	4800	4800	4800
$\left(\varsigma_{22}^p\right)_{33}/\left(kg\cdot m^{-3}\right)$	-1125	-1125	-1125
$c_{44}^p/\left(N\cdot m^{-2}\right)$	22.2×10^9	23.0×10^9	25.0×10^9
$e_{15}^p/\left(C\cdot m^{-2}\right)$	9.8	17.0	13.5
$\zeta_{15}^p/\left(C\cdot m^{-2}\right)$	4.20	7.80	6.56
$\theta_{11}^p/\left(F\cdot m^{-1}\right)$	5.2×10^{-9}	11.2×10^{-9}	10.8×10^{-9}
$\lambda_{11}^p/\left(F\cdot m^{-1}\right)$	8.76×10^{-9}	27.70×10^{-9}	17.10×10^{-9}
$\lambda_{11}^{pp}/\left(F\cdot m^{-1}\right)$	10.90×10^{-9}	29.90×10^{-9}	21.80×10^{-9}

Table2
Material constants for heterogeneous half space. [14]

Parameter/Material	Isotropic heterogeneous half pace
$\mu/\left(N.m^{-2}\right)$	23.24×10^{10}
$\varsigma_2/\left(kg\cdot m^{-3}\right)$	5.008×10^3

Graphs have been plotted to represent the variation of dimensionless phase velocity (c) and group velocity $\left(c_g\right)$ against dimensionless wave number and have shown by Figs. 2-11. Fig. 12 represents the surface plot by taking the group velocity, dimensionless wave number and width of porous piezoelectric layer in three axes. Moreover, Fig. 13 is drawn to show the comparison between phase and group velocity.

Fig.2 reveals the influence of piezoelectric constant on phase velocity of SH waves. It is observed that increase of piezoelectric constant (in fashion of arithmetic progression with common difference of $5C/m^2$) decreases the phase velocity. This theoretical result can be used to regulate the efficiency of sensors involving piezoelectric materials. Fig. 3 represents the effect of elastic constant on the dimensionless phase velocity. It is observed that as we increase the value of elastic constant (in fashion of arithmetic progression with common difference of $5N/m^2$) the phase velocity decreases.
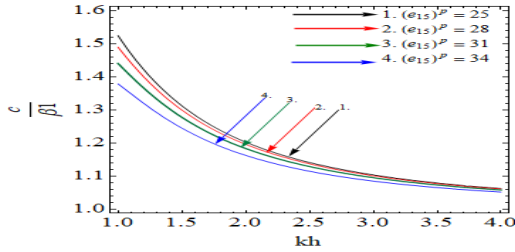
Fig.2
Variation of dimensionless phase velocity against dimensionless wave number for different values of piezoelectric constant.
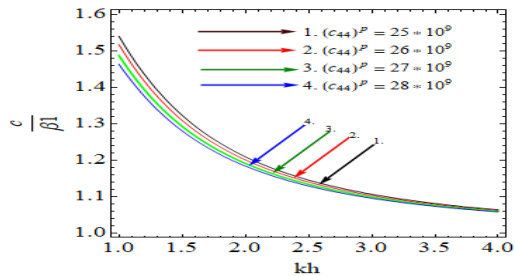
Fig.3
Variation of dimensionless phase velocity against dimensionless wave number for different values of elastic constant.

Figs. 4 and 5 represent the prominent influence of initial stress parameter of porous piezoelectric medium on dimensional phase velocity and group velocity of SH waves respectively.

It is observed from Fig. 4 that increment in initial stress parameter decreases the dimensionless phase velocity of SH waves. The curves of Fig. 5 signify the variation of group velocity against wave number.
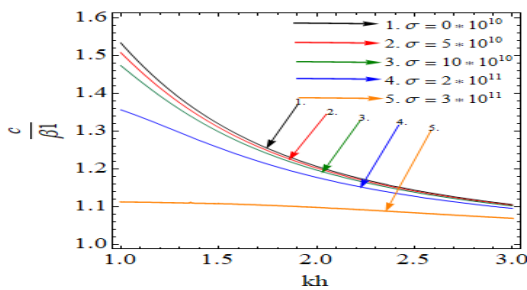
Fig.4
Variation of dimensionless phase velocity against dimensionless wave number for different values of initial stress.
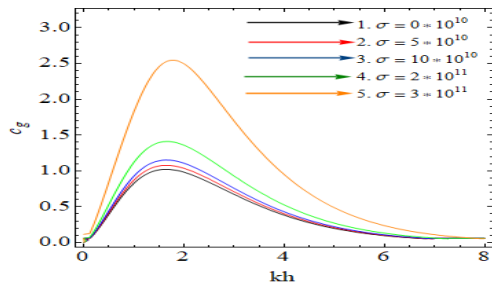

Fig.5
Variation of dimensionless group velocity against dimensionless wave number for different values of initial stress.

The substantial influence of the thickness of the porous piezoelectric layer on the phase velocity and group velocity has been shown through Figs. 6 and 7 respectively. There is a remarkable finding in Fig. 6 that as we increase the value of width of the layer the dimensionless phase velocity of SH wave increases. This result may be useful for fixing the plate (porous piezoelectric) width of sensors and seismic devices, used for seismic recording in high-frequency range.
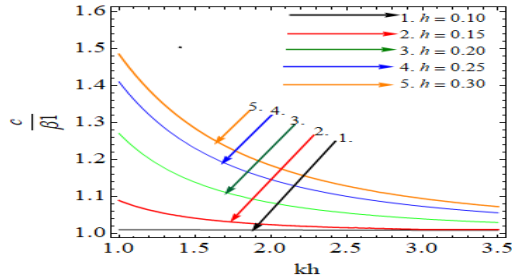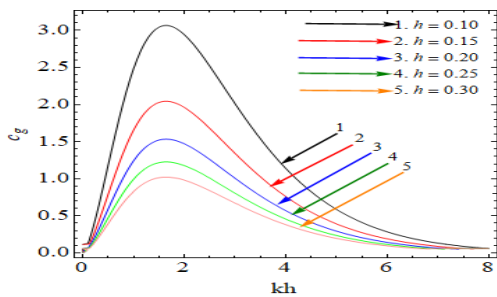

Fig.6
Variation of dimensionless phase velocity against dimensionless wave number for different values of layer width (porous piezoelectric layer).

Fig.7
Variation of dimensionless group velocity against dimensionless wave number for different values of layer width (porous piezoelectric layer).

Fig. 8 reveals the influence of heterogeneity parameter (γ) associated with the heterogeneous half-space on the dimensionless phase velocity of SH wave. It is observed that the dimensionless phase velocity decreases with increase in the value of heterogeneity parameter (γ).

Variation of dimensionless phase velocity against dimensionless wave number for different porous-piezoelectric materials is shown in Fig. 9, when the layer is composed of PZT-7, PZT-5H and PZT-1 materials. The highest value of phase velocity is found in the case of PZT-7H following the PZT-1 and PZT-5. Phase velocity is found to be comes closer in the case of PZT-7 and PZT-5H materials
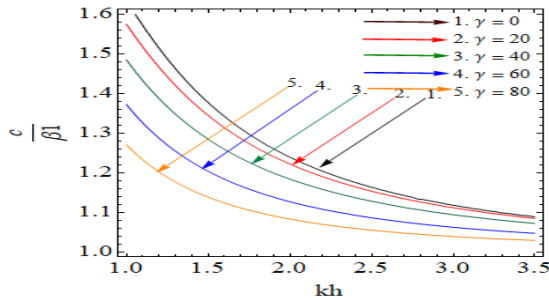

Fig.8
Variation of dimensionless phase velocity against dimensionless wave number for different values of heterogeneity parameter (for lower heterogeneous half space).
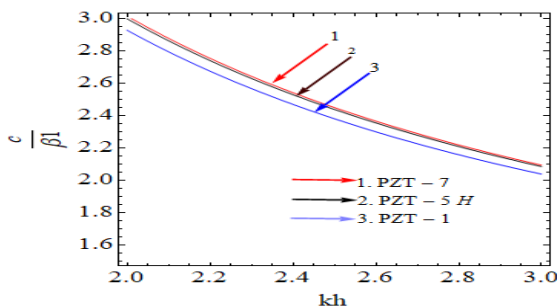

Fig.9
Variation of dimensionless phase velocity against dimensionless wave number for different values of material constants (porous-piezoelectric material).

From Fig.10, it can be observed that the phase velocity of the SH wave increases due to the porosity in the piezoelectric materials. The similar effect we can find in Fig. 11. Fig. 12 represents the surface plot among the group velocity, dimensionless wave number and width of porous piezoelectric layer.

Fig. 13 demonstrate the comparison between phase velocity and group velocity. The group velocity is found less than the phase velocity hence we call the dispersion as 'normal'.
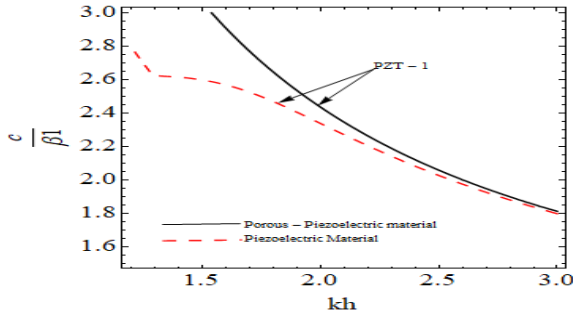

Fig.10
Comparison of dimensionless phase velocity against dimensionless wave number for porous piezoelectric material and piezoelectric material.
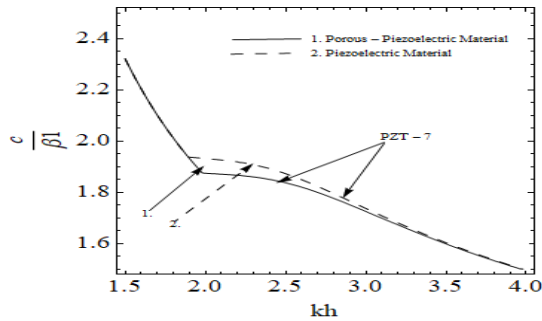

Fig.11
Comparison of dimensionless phase velocity against dimensionless wave number for porous piezoelectric material and piezoelectric material.
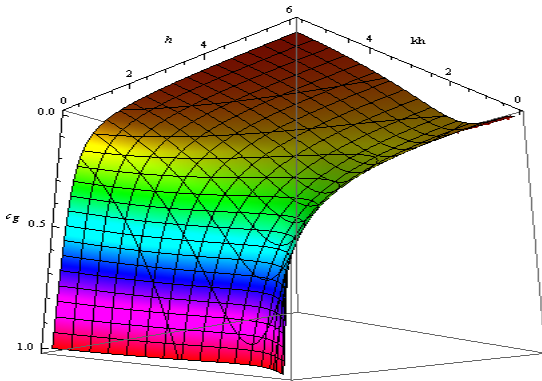

Fig.12
Surface plot by taking the group velocity, dimensionless wave number and width of porous piezoelectric layer in three axes.
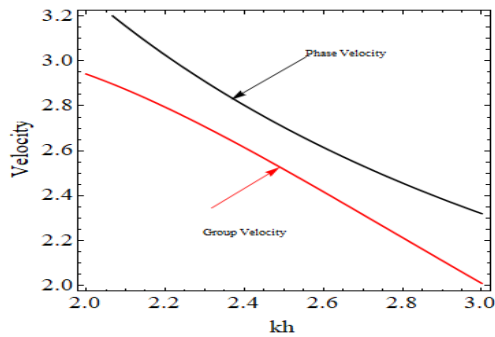

Fig.13
Comparison of dimensionless phase velocity and group velocity against dimensionless wave number.

8   POSSIBLE APPLICATION

Lead Zirconate Titanate (PZT) is one of the most excellent executing, cost price effective piezoelectric materials. High piezoelectric responses depends on dense ceramics, to achieve that, porosity generally causes for reducing mechanical and piezoelectric properties respectively. In order to minimize this problem, the Nb ions codoped with PZT material to control the large porous microstructure. Consequently, the codoped material becomes a new crucial applicative entrant for the vibrant applications in the field of ultrasonic transducer. Into the form of 2-phase composite, the porous ceramic can be visualized. These ceramic materials are highly utilized because of having more advantages such as specific electronic properties, high melting point, low thermal mass, low thermal conductivity. The performance of this material may further be enhanced by incorporation of appropriate porosity.
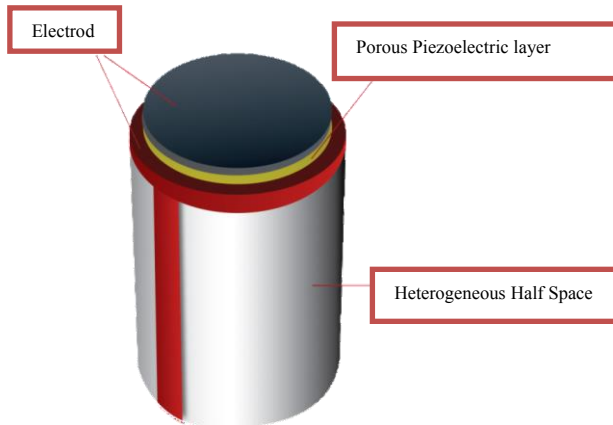

Electrod

Porous Piezoelectric layer

Heterogeneous Half Space

Fig.14
(a) Single element thick film transducer.

Top Electrode (Silver)

Active piezoelectric element (Porous-Piezo layer)

Bottom Electrode (Gold)

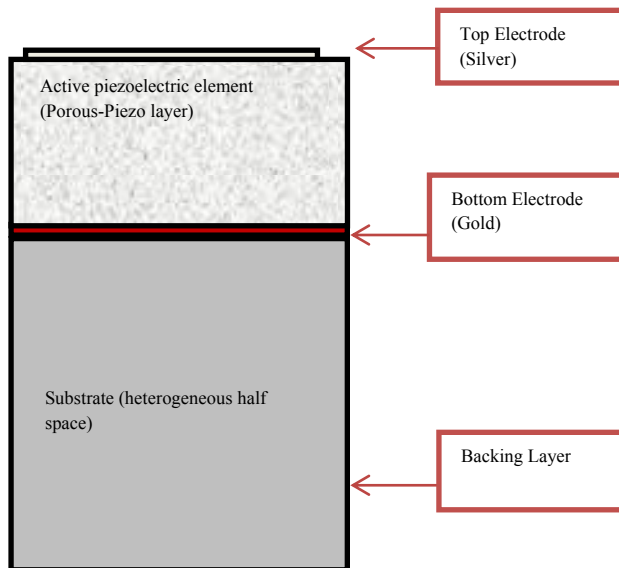Substrate (heterogeneous half space)

Backing Layer

Fig.14
(b) Multi element array transducer.

However, due to the poor acoustic coupling to the media and low hydrostatic figure of merit (FOM) so the dense PZT-type piezo-ceramics are not suitable for these applications. That's why the porous materials has got significant applications in various scientific areas such as in cleanliness and filtration of molten metals, support for catalytic reactions, high-temperature thermal insulation, and filtration of hot caustic gases in industrial window. It is also utilized as ultrasonic transducers. Due to the generation of intense ultrasonic wave the ultrasonic transducers may be useful for high penetration, erosion of paints, welding and also as medical diagnostic instruments. The displacement among the atoms around the equilibrium positions starts due to the propagation of ultrasonic waves in the material. Subsequently, the force raised due to mechanical vibrations of atoms creates stress-strain interactions inside the typical structure of material. This wave may propagate into the form of longitudinal waves, shear waves, Rayleigh

waves and Lamb waves. In general, the longitudinal waves are used as ultrasonic waves. In this system displacements between two atoms of piezo-ceramic transducers are created using high frequency. The term of transmitter or receiver is basically part of active piezoelectric element which is formed from a piezo-ceramics disk such as 1 to 2 cm wide, where two different electrodes are created on both sides for biasing purpose. After applying a sufficient voltage on these electrodes the depletion layer enhances due to the variation of the transducer. Here, the mechanism of inverse piezoelectric effect takes place. In addition to this, the backing layer works to provide a mechanical support for active element and attenuate the acoustic energy from back to back face of transducer. This is worth to note that the backing and active layer materials should be similar impedance rates for the optimization of transmission of the ultrasounds. To achieve this condition epoxy resins incorporated along with tungsten particles are utilized as substances for backing layers purpose.

9 CONCLUSIONS

The influence of heterogeneity, piezoelectric constants, initial stress, layer's width and elastic constants on the dispersion of SH-wave in a porous piezoelectric layer overlying by a heterogeneous substrate under point source scheme was investigated. Numerical example has been shown for three distinct types of piezoelectric materials (namely PZT-5H, PZT-7 and PZT-1) and the influence of affecting parameters on dispersion curves were illustrated by graphs. The outcomes of the study are as follows:

1. The phase velocity of SH-wave is found to have decreasing nature with respect to wave number
1. Influence of heterogeneity parameter, piezoelectric and elastic constants has significant impact on the phase velocity curve.
2. In PZT-5H material phase velocity is high in comparison with PZT-1 and PZT-7.
3. Some of the results (in particular influence of layer's width and influence of initial stress on phase velocity and group velocity of considered wave) suggests for selection of a suitable porous piezoelectric material in devices like transducers, rotating sensors and SAW device in order to prevent the brittle fracture.
4. Obtained result is validated by matching the obtained dispersion relation with the classical Love wave equation.

ACKNOWLEDGMENTS

REFERENCES

[1]   Ezzin H., Amor M.B., Ghozlen M.H.B., 2017, Propagation behavior of SH waves in layered piezoelectric/piezomagnetic plates, *Acta Mechanica* **228**(3): 1071-1081.
[2]   Ezzin H., Amor M.B., Ghozlen M.H.B., 2017, Lamb waves propagation in layered piezoelectric/piezomagnetic plates, Ultrasonics **76**: 63-69.
[3]   Alam P., Kundu S., 2017, Influences of heterogeneities and initial stresses on the propagation of love-type waves in a transversely isotropic layer over an inhomogeneous half-space, *Journal of Solid Mechanics* **9**(4): 783-793.
[4]   Sahu S.A., Singhal S., Chaudhary S., 2017, Influence of heterogeneity on Rayleigh wave propagation in an incompressible medium bonded between two half-spaces, *Journal of Solid Mechanics* **9**(3): 555-567.
[5]   Sahu S.A., Singhal A., Chaudhary S., 2017, Surface wave propagation in functionally graded piezoelectric material: An analytical solution, *Journal of Intelligent Material Systems and Structures* **29**: 423-437.
[6]   Kumar R., Gupta R.R., 2010, Study of wave motion in an anisotropic fiber-reinforced thermoelastic solid, *Jounral of Solid Mechanics* **2**(1): 91-100.
[7]   Chaudhary S., Sahu S., Singhal A., 2017, Analytic model for Rayleigh wave propagation in piezoelectric layer overlaid orthotropic substratum, *Acta Mechanica* **228**(2): 495-529.
[8]   Singhal A., Sahu S.A., Chaudhary S., 2018, Liouville-Green approximation: An analytical approach to study the elastic waves vibrations in composite structure of piezo material, *Composite Structures* **184**: 714-727.
[9]   Kumar V., Jiwari R., Kumar G. R., 2013, Numerical simulation of two dimensional quasilinear hyperbolic equations by polynomial differential quadrature method, *Engineering Computations* **30**(7): 892-909.

[10] Verma A., Jiwari R., 2015, Cosine expansion based differential quadrature algorithm for numerical simulation of two dimensional hyperbolic equations with variable coefficients, *International Journal of Numerical Methods for Heat & Fluid Flow* **25**(7): 1574-1589.

[11] Ghosh M.L., 1963, On love waves across the ocean, *Geophysical Journal International* **7**(3): 350-360.

[12] Chattopadhyay A., Singh A.K., 2011, Effect of point source and heterogeneity on the propagation of magnetoelastic shear wave in a monoclinic medium, *International Journal of Engineering, Science and Technology* **3**(2): 68-83.

[13] Chattopadhyay A., Gupta S., Kumari P., Sharma V., 2012, Effect of point source and heterogeneity on the propagation of SH-waves in a viscoelastic layer over a viscoelastic half space, *Acta Geophysica* **60**(1): 119-139.

[14] Chattopadhyay A., Kar B.K., 1981, Love waves due to a point source in an isotropic elastic medium under initial stress, *International Journal of Non-Linear Mechanics* **16**(3-4): 247-258.

[15] Singh A.K., Das A., Ray A., Chattopadhyay A., 2018, On point source influencing Love-type wave propagation in a functionally graded piezoelectric composite structure: A Green's function approach, *Journal of Intelligent Material Systems and Structures* **29**(9): 1928-1940.

[16] Singhal A., Sahu S.A., Chaudhary S., 2018, Approximation of surface wave frequency in piezo-composite structure, *Composites Part B: Engineering* **144**: 19-28.

[17] Chaudhary S., Sahu S.A., Dewangan N., Singhal A., 2018, Stresses produced due to moving load in a prestressed piezoelectric substrate, *Mechanics of Advanced Materials and Structures* **26**(12): 1028-1041.

[18] Othmani C., Takali F., Njeh A., Ghozlen M.H.B., 2017, Numerical simulation of Lamb waves propagation in a functionally graded piezoelectric plate composed of GaAs-AlAs materials using Legendre polynomial approach, *Optik-International Journal for Light and Electron Optics* **142**: 401-411.

[19] Othmani C., Takali F., Njeh A., 2017, Investigating and modeling of effect of piezoelectric material parameters on shear horizontal (SH) waves propagation in PZT-5H, PMN-0.33 PT and PMN-0.29 PT plates, *Optik-International Journal for Light and Electron Optics* **148**: 63-75.

[20] Borodina I.A., Zaitsev B.D., Kuznetsova I.E., Teplykh A.A., 2013, Correspondence-Acoustic waves in a structure containing two piezoelectric plates separated by an air (vacuum) gap, *IEEE Transactions on Ultrasonics, Ferroelectrics, and Frequency Control* **60**(12): 2677-2681.

[21] Kuznetsova I.E., Zaitsev B.D., Joshi S.G., Borodina I.A., 2001, Investigation of acoustic waves in thin plates of lithium niobate and lithium tantalate, *IEEE Transactions on Ultrasonics, Ferroelectrics, and Frequency Control* **48**(1): 322-328.

[22] Vashishth A.K., Gupta V., 2009, Vibrations of porous piezoelectric ceramic plates, *Journal of Sound and Vibration* **325**(4-5): 781-797.

[23] Kumar R., Hundal B.S., 2009, Surface wave propagation in a fluid-saturated incompressible porous layer lying between an empty porous elastic layer and an empty elastic porous half-space, *Journal of Porous Media* **12**(5): 387-402.

[24] Vashishth A.K., Gupta V., 2015, 3-D waves in porous piezoelectric materials, *Mechanics of Materials* **80**: 96-112.

[25] Chaudhary S., Sahu S.A., Singhal A., 2018, On secular equation of SH waves propagating in pre-stressed and rotating piezo-composite structure with imperfect interface, *Journal of Intelligent Material Systems and Structures* **29**(10): 2223-2235.

[26] Baroi J., Sahu S.A., Singh M.K., 2018, Dispersion of polarized shear waves in viscous liquid over a porous piezoelectric substrate, *Journal of Intelligent Material Systems and Structures* **29**(9): 2040-2048.

[27] Pan E., Han F., 2004, Green's functions for transversely isotropic piezoelectric multilayered half-spaces, *Journal of Engineering Mathematics* **49**(3): 271-288.

[28] Singh A.K., Lakshman A., Mistri K.C., Pal M.K., 2018, Torsional surface wave propagation in an imperfectly bonded corrugated initially-stressed poroelastic sandwiched layer, *Journal of Porous Media* **21**(6): 499-522.

[29] Shodja H.M., Eskandari S., Eskandari M., 2016, Shear horizontal surface acoustic waves in functionally graded magneto-electro-elastic half-space, *Journal of Engineering Mathematics* **97**(1): 83-100.

[30] Kong Y., Tian R., Xu J., Liu J., 2018, Propagation behavior of SH waves in a piezomagnetic substrate with an orthorhombic piezoelectric layer, *Applied Mathematics and Mechanics* **39**(2): 207-218.

[31] Chattopadhyay A., Pal A.K., Chakraborty M., 1984, SH waves due to a point source in an inhomogeneous medium, *International Journal of Non-Linear Mechanics* **19**(1): 53-60.

[32] Vashishth A.K., Dahiya A., Gupta V., 2015, Generalized bleustein-gulyaev type waves in layered porous piezoceramic structure, *Applied Mathematics and Mechanics* **36**(9): 223-242.